Two-beam interference patterning of biodegradable magnesium alloy: Influence of number of passes and spots overlap

Valentina Furlan, Marco Biondi, Ali Gökhan Demir, Barbara Previtali, Giorgio Pariani, and Andrea Bianco

Citation: Journal of Vacuum Science & Technology B, Nanotechnology and Microelectronics: Materials, Processing, Measurement, and Phenomena **36**, 01A102 (2018); doi: 10.1116/1.4996504

View online: http://dx.doi.org/10.1116/1.4996504

View Table of Contents: http://avs.scitation.org/toc/jvb/36/1

Published by the American Vacuum Society

Two-beam interference patterning of biodegradable magnesium alloy: Influence of number of passes and spots overlap

Valentina Furlan,[a] Marco Biondi, Ali Gökhan Demir, and Barbara Previtali
Department of Mechanical Engineering, Politecnico di Milano, Via La Masa 1, 20156 Milan, Italy

Giorgio Pariani and Andrea Bianco
INAF, Osservatorio Astronomico di Brera, Via E. Bianchi 46, 23807 Merate, Lecco, Italy

(Received 17 July 2017; accepted 11 September 2017; published 12 October 2017)

Laser based texturing methods provide enhanced surface properties exploitable, especially in biomedical applications. Direct writing methods allow for processing features in tens of micrometers in size due to the use of diffraction limited beams. Feature size can be further reduced exploiting the light interference combined with the pulsed laser ablation. In this work, an industrial grade single mode nanosecond-pulsed green fiber laser was used to realize two-beam direct laser interference patterning system. The system was employed on a biodegradable Mg alloy to test the feasibility of the approach for submicrometric patterning. The combination of low melting point and high thermal conductivity of Mg alloy with the use nanosecond pulses generates difficulties in terms of the machining quality. The influence of number of pulses and number of passes was evaluated on the patterned area diameter as well as the pattern periodicity. Finally, patterned regions were overlapped on a scanned line to assess the feasibility of the process on larger areas. © *2017 American Vacuum Society*. https://doi.org/10.1116/1.4996504

I. INTRODUCTION

Surface texturing is an attractive tool applied in different fields, from automotive to biomedicine, in order to produce controllable micrometric features on relatively large surface areas. In spite of the large number of texturing methods, those based on the use of high power lasers are widely employed thanks to highly flexible, noncontact, and single step processing. Among different laser techniques, direct laser writing is the most common one with the minimum feature size in the order of few micrometers due to the use of diffraction limited beams.[1] On the other hand, further reduction of feature size to nanometric scale and a hierarchical use of micro- to nanofeatures enable further possibilities in tailoring the surface properties.[2] The production of periodic surface structures is possible through several techniques such as lithography and replica molding. However, these techniques require multiple steps and involve artifact issues.[3,4] Ultrashort pulsed laser source can be used with direct laser writing to induce naometric ripple formation.[5] Hierarchical structures are also achievable with a defined direction and period; unfortunately, the ripple formation is difficult to control in terms of size variation. A relatively recent laser texturing technique is direct laser interference patterning (DLIP). DLIP is based on interference phenomena that occurs when two or more coherent laser beams are recombined at the same point with a defined phase difference. In this way, controlled features in the micro- and nanometer range can be obtained.[3] The number of interfering beams and the angle between them determine the shape and dimension of the periodic pattern.[3,4]

To this date, different materials were investigated using DLIP method, ranging from polymers to metals.[6,7] Pulsed laser sources with different pulse duration and wavelength were studied in order to determine laser parameters' effect on the realized pattern.[8,9] In particular, feature quality and size, which are crucial in biomedical applications, were investigated as function of laser fluence and number of pulses.[9–13]

Surface texture in micro- and nano level as well as chemistry should be controlled to tailor the biological performance of the implant.[14] Hence, laser surface texturing of implant materials has received a great deal of attention from scientific communities, mainly concentrating on permanent implant materials such as stainless steel,[15] Ti-alloys,[16] and CoCr alloys.[17] More recently, the scientific communities have focused their attention toward biodegradable metals as implant materials for temporary grafting.[18,19] The applications range from cardiovascular stents to orthopedic implants.[18,20] For all these applications, surface texture plays an important role for controlling the interaction between the implant and the surrounding environment. Several surface treatments have been proposed for Mg alloys employing lasers. These treatments were concentrated mainly on the improvement of the corrosion rate,[21–25] optical properties,[26,27] and tribological behavior.[28,29] On the other hand, laser surface texturing of Mg alloys has been investigated for controlling surface wettability, which is fundamentally important for biological performance of the implant.[30,31] The use of direct writing with a laser beam also demonstrated for producing submicrometric and stochastic surface structures on the Mg alloy surface.[32]

On the other hand, DLIP stands out as a flexible option for generating periodic and deterministic surface structures in submicrometric scale on biodegradable Mg alloys. However, these materials show critical aspects due to high reactivity, low melting temperature, and high thermal conductivity.[33,34] The periodic structure formation can be

[a]Electronic mail: valentina.furlan@polimi.it

obscured due to high melt fraction and surface oxidation within the process.

In this work, the processability of AZ31 magnesium through DLIP is investigated. The DLIP process was applied with a single mode green pulsed fiber laser in a two-beam configuration. In particular, the high beam quality, low energy content, and high repetition rate of this source are novel aspects compared to the more commonly applied laser sources with lower repetition rates and higher energy levels. The laser source lends itself to more common micromachining applications based on multiple passes and high speed scanning. Such possibilities should be investigated for DLIP, especially for covering relatively large areas. Moreover, the inability of single pulse control in industrial fiber laser, which are characterized by a train pulse profile, can strongly affect the process. From this point of view, this work investigates the influence of main process parameters (fluence and number of pulses) on pattern quality was analyzed. Patterning was applied on single spots as well as on lines, demonstrating a first step to the feasibility for larger area processing.

II. EXPERIMENT

A. Employed material

Treatments were performed on AZ31 magnesium alloy (Goodfellow, Huntingdon, UK). Cold rolled sheets of 0.2 mm thickness was cut in rectangular samples of 10 × 10 mm^2, sonicated in acetone bath for 10 min before treatment. The alloy is characterized by a melting temperature at 905 K and a vaporization temperature at 1363 K.[35]

B. DLIP setup

DLIP treatments were performed with a single mode nanosecond-pulsed green fiber laser, with a maximum average power of 6 W, a pulse duration of 1.2 ns, and an emission wavelength of 532 nm (YLPG-5, by IPG Photonics, Oxford, MA). The source was based on a master oscillator power amplifier (MOPA) architecture. Low energy pulses were generated at 1 μm wavelength, transferred to a remote amplifier with a delivery fiber, amplified at this point and converted to 532 nm. The high beam quality is maintained with low ns pulse duration at relatively low pulse energy levels (20 μJ). The main characteristics of employed laser source are summarized in Table I. The laser was characterized by a ramped pulse profile. At the initial part of the laser emission, the pulse train shows an increasing energy trend, which then stabilizes after approximately 40 pulses.

TABLE I. Main characteristics of employed laser source.

Parameter	Symbol	Value
Wavelength	λ	532 nm
Pulse duration	τ	1.2 ns
Pulse repetition rate	PRR	20–300 kHz
Beam quality factor	M^2	1.12
Maximum average power	P_{ave}	6 W
Collimated diameter	d_c	3.49 mm

Figure 1 depicts the developed DLIP setup, which is based on Mach–Zehnder interferometer. The laser produced a collimated beam in the output, which is linearly polarized. The beam is split in two by means of a beam splitter. Two mirrors are used to deflect the split laser beams on the sample plane and set the desired interference angle (θ). The two deflected beams are then focused on the target point using two lenses with a 100 mm focal length. Sample positioning was carried out with manual micrometric axis.

C. Experimental design

Following the results of preliminary work,[36] DLIP was applied with fixed pulse repetition rate (PRR), focal position, and interference angle. These parameters were set to lower the energy density over the processing zone in order to apply a superficial ablation process. All experiments were carried out in ambient atmosphere. The expected period with the employed 26° interference angle is 1.18 μm. This large period was chosen at this stage of the work in order to assess the feasibility of the process. In the first stage of the work, the number of pulses (N) in the ramped pulse train was varied. This resulted in a change of average pulse energy (E_m) due to the ramped emission profile. SEM images of the treated regions were acquired morphology (EVO-50 from Carl Zeiss, Oberkochen, Germany). Ablated region diameter (D) and pattern periodicity (Λ) were measured over the images. The experimental conditions are summarized in Table II. The results were evaluated as a function of mean fluence, which was calculated from the following equation:

$$F_m(N) = \frac{2E_m(N)}{\pi w_s^2}, \quad (1)$$

where $E_m(N)$ is the mean energy of the pulse train composed of N number of pulses, and w_s radius of laser beam at the surface of the material. In the second stage, the effect of multiple passes (P) over the same irradiated zone was assessed. Single and four passes were evaluated. In the last phase, the processing was evaluated to test overlapping between adjacent irradiated zones over a scanned line to assess the feasibility of processing larger areas. Surface chemical composition was assessed using energy dispersive

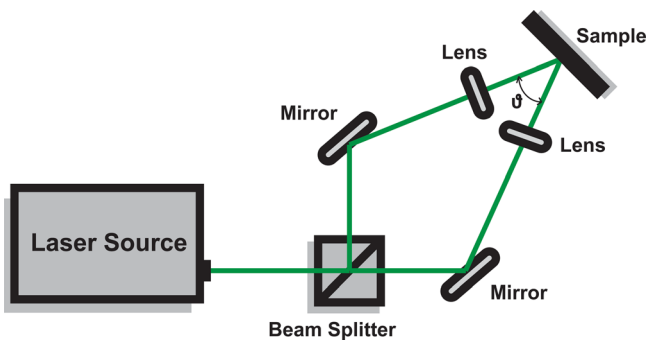

FIG. 1. (Color online) Schematic representation of the DLIP set-up.

TABLE II. Fixed and varied parameters in the experimental work.

Fixed parameters	
Pulse energy in regime, E_{st} (μJ)	20
Pulse repetition rate, PRR (kHz)	20
Focal position, Δz (mm)	2.5
Spot size on surface, d_s (μm)	91
Interference angle, θ (deg)	26
Varied parameters	
Number of pulses, N	17, 25, 34, 44, 54, 64
Number of passes, P	1, 4

x-ray spectroscopy (EDS, Inca Energy 200 from Oxfod Instruments, Abingdon, UK). The sensing depth of the instrument was 5 μm. For pointwise measurements, the sesnig area was a circular region with 2 μm.

III. MODELING

A. Interference model

In two-beam interference the intensity distribution can be expressed as[37]

$$I = I_1 + I_2 + 2\sqrt{I_1 \cdot I_2}\cos(\varphi), \tag{2}$$

where I_1 and I_2 are the intensities of first and second beams, respectively, $\varphi = (2\pi r/\Lambda)$ is the phase difference between two beams, r is the distance from spot center, and Λ is the fringe period. For a case where interfering beams are slip with equal intensities $I_1 = I_2$, it is possible obtain

$$I = 2 \cdot I_1[1 + \cos(\varphi)]. \tag{3}$$

Figures 2(a)–2(c) compare the energy distributions of a single Gaussian beam and two interfering beams with different angles. It can be seen that the energy content is modulated generating a fringe pattern, which is employed to produce the periodic surface structures. It should be noted that the interfering beams follow the native Gaussian distribution with the superimposed fringe pattern. Accordingly, toward the beam center the energy density is higher. From an operative point of view, the fringe period [Λ (μm)] is determined by the interference angle [θ (°)] and the laser wavelength [λ (μm)] by the following equation:

$$\Lambda = \frac{\lambda}{2\sin\left(\frac{\theta}{2}\right)}. \tag{4}$$

IV. RESULTS AND DISCUSSION

A. Effect of number of pulses

Figure 3 shows the mean laser fluence values as function of the number of pulses and the corresponding SEM images of the treated surfaces. It can be seen that the resulting fluence values vary between 0.3 and 0.9 J/cm^2. Figure 4 depicts the diameter of the treated region and pattern periodicity as a function of number of pulses. An increase in fluence is

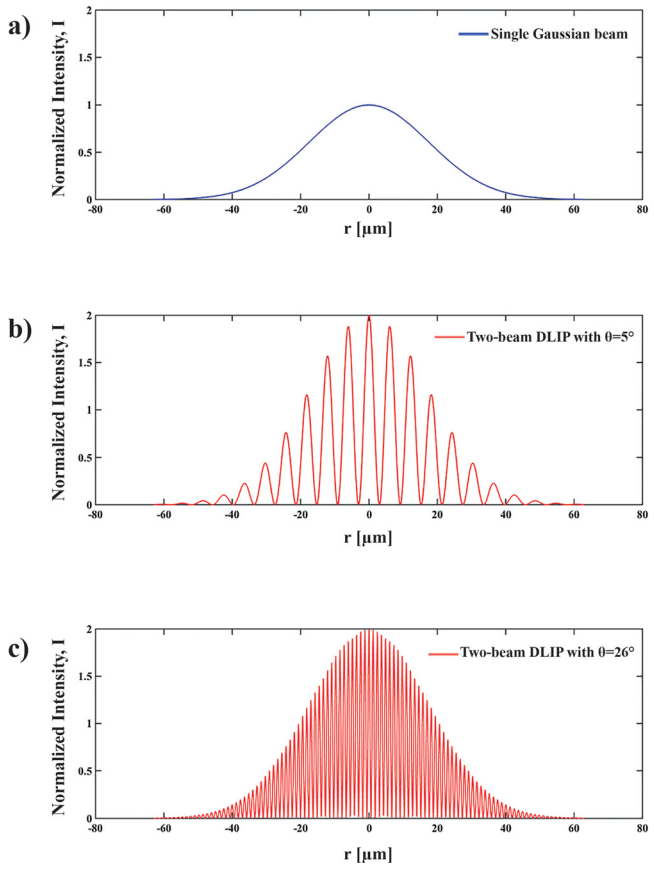

FIG. 2. (Color online) (a) Energy distribution of a single Gaussian beam. (b) Energy distribution of two interfering beams with a $\theta = 5°$. (c) Energy distribution of two interfering beams with a $\theta = 26°$.

associated with an increased treated region diameter, ranging from 36 to 71 μm in correspondence to the highest fluence level. The treated region size is smaller than the theoretical value of the spot diameter on the material surface in all the experimented conditions.

The use of higher fluence can further increase the diameter of the ablated region; however, the process is accompanied by high formation of melt and closure of the periodic structures.

On the other hand, fluence also affected pattern quality. Lower fluence values resulted in a smaller and nonhomogeneous patterned area. Increased fluence induced wider ablated area and better defined patterns. Fringe period was measured was found to not vary as a function of the number of pulses and measured to be $\Lambda = 1.32 \pm 0.03$ μm.

The measured periodicity is approximately 0.14 μm higher than the theoretical value. This can be attributed to the error in the positioning of the two beams, hence an error of approximately 2°. In terms of fringe quality and pattern definition, processing with N = 64 proved to be the best solution, which was further analyzed in the next steps.

B. Effect of multiple passes

Figures 5(a) and 5(b) show the SEM images of patterned surfaces obtained with a single pass and using N = 64. In both cases, the surface pattern is clearly visible, but pattern

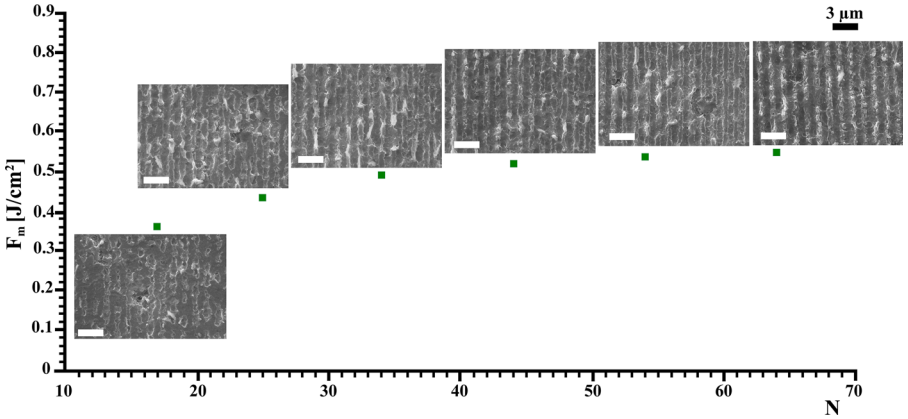

FIG. 3. (Color online) SEM images of the patterned surfaces as a function of number of pulses, N, in the ramped emission profile and mean fluence F_m.

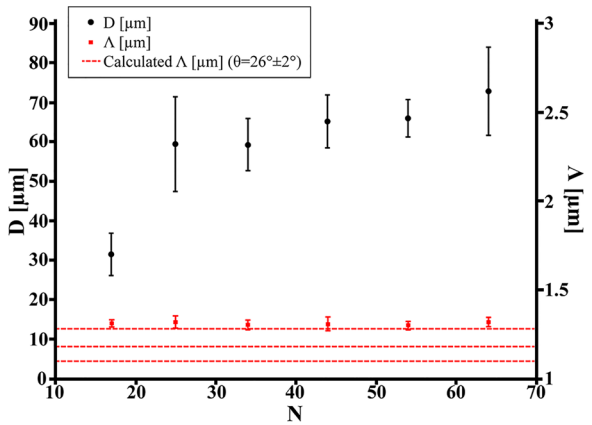

FIG. 4. (Color online) Patterned region diameter (D) and periodicity (Λ) as a function of number of pulses (N).

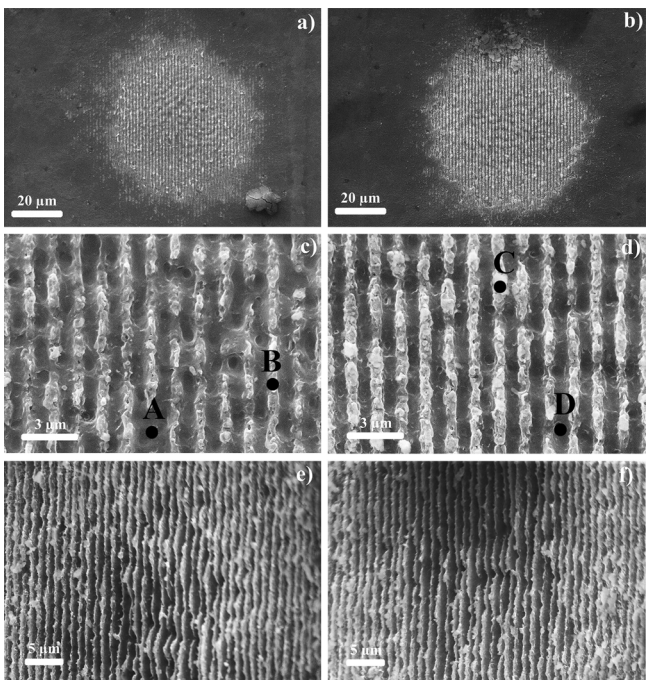

FIG. 5. SEM images of patterned surfaces with a single pass [(a), (c), and (e)] and four passes [(b), (d), and (f)]. In (a)–(d), the SEM top-view acquisition. In (e) and (f), the side-view acquisition realized with a tilt angle equal to 45°. Laser parameters are E = 20 J, PRR = 20 kHz, $\theta = 26°$, and N = 64.

definition is improved by the multiple passes. As indicated in Fig. 5(c), the periodic pattern is interrupted over the single lines. Molten and resolidified regions are visible. The use of multiple passes corresponds to repeating the same pulse train by interrupting the process between the pulse trains. Similar to multiple passes in laser engraving, this strategy allows for material transport in between different passes and avoids material heat-up compared to a longer pulse train without any interruptions.

Figures 5(c) and 5(d) show that the fringe quality is improved and the interrupted regions are avoided by the multiple passes. Overall, the structure periodicity is maintained and the structures appear deeper. Figures 5(e) and 5(f) show the patterned surface from an inclined view. Both the images confirm an effective machining in depth and a regular pattern periodicity. In both cases over the pattern ridges traces, molten and resolidified material is observed.

Indeed, the melting and resolidification phenomenon in ambient atmosphere may result in oxidation. In the case of treating a highly reactive metal such as a Mg-alloy, surface oxidation is almost investable. However, the DLIP process possesses its own peculiarity in terms of a selective ablation mechanism in submicrometric to a few micrometers region over a large area that is between tens of micrometers to milimeters. Table III reports the EDS analysis on the base material and DLIP treated region. A general comparison between the base material and an overall treated region shows similar results, where alloying element levels remain almost unvaried and surface oxide levels are comparable. Analyzing different regions of a DLIP treated area shows a more interesting behavior. Regions of material removel

TABLE III. EDS analysis results.

wt. %	Mg	O	Al	Zn
Base material	91.1	4.5	3.5	0.9
DLIP surface	91.3	5.0	2.9	0.8
A	94.4	2.3	2.4	0.9
B	87.4	8.4	3.6	0.6
C	78.2	18.0	3.0	0.8
D	95.1	1.8	2.3	0.8

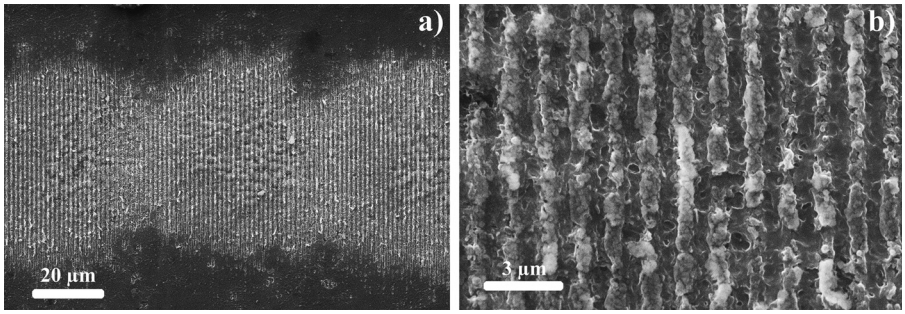

FIG. 6. Adjacent laser treatment spots to evaluate the feasibility of large area treatments: (a) partial overlap of three spots and (b) SEM image of the overlapped area. Laser parameters are E = 20 μJ, PRR = 20 kHz, θ = 26°, and N = 64.

achieved both with a single pass (A) and four passes (D) show reduced levels of oxidation (see Fig. 5 and Table III). A completely opposite behavior is observed at regions where material removal did not occur (B, C). More interestingly, the alloying content of allotting elements (Al and Zn) appear almost unvaried. Apparently, the DLIP process generates preferential oxidation, where destructive interference regions are enriched with oxygen and its content rises with increased number of passes. Although in many applications surface oxidation can be regarded as a defect, such feature of DLIP can be exploited for tailoring the chemical properties along with the surface structure. The presence of MgO has shown to slow down corrosion.[38] The use of periodically oxided regions can be useful also for controlling the corrosion direction.

C. Overlapping between treated regions

For processing large areas overlapping is a crucial point. However, the periodicity of the interference pattern renders the overlapping between different regions an issue. Indeed, overlapping along the periodic direction of the pattern is more problematic due to the correct alignment between the treated areas. Multiple passes on the single ablated region adds up to the complexity of the problem. Accordingly, the feasibility of treating the surfaces by overlapping the treated regions along the periodic direction was assessed. Treatment was realized using previously selected condition (E = 20 μJ, PRR = 20 kHz, θ = 26°, and N = 64) with a single pass. The ablated zone diameter was 71 μm. In order to guarantee an overlapped zone of 20 μm, the distance between two consecutive treatments was set to 50 μm.

Figure 6(a) shows the adjacent treated regions over the scanned line. Figure 6(b) shows a magnification of the overlapping zone between two spots, which represented the critical point for a good and continuous pattern generation. The resulted pattern maintained good quality and the same period value estimated previously.

V. SUMMARY AND CONCLUSIONS

This work demonstrated the use of DLIP on a biodegradable Mg alloy for submicrometric to nanometric surface patterning. The main conclusions can be listed as follows:

(1) The process feasibility requires limited amount of laser fluence for the clear formation of periodic structures. The increase of laser fluence to around 0.9 J/cm^2 was found to also improve pattern definition, whereas a further increase was found to generate excessive melt.
(2) Pattern quality could be improved using multiple passes. Instead of increasing fluence or higher number of pulses, which can deteriorate the periodic structure definition, the strategy was found to eliminate the interruptions over the structured lines and to be repeatable.
(3) Patterned regions showed an overall similar chemical composition to the nontreated alloy surface. However, different regions under constructive and destructive interference were characterized by different oxidation levels implying the possibility of tailoring the surface chemistry within the process.
(4) Treated regions were applied over a line with partial overlapping. The periodic structures were found to be stable and well defined in the overlapping region.
(5) Pattern periodicity did not depend on any of the process parameters except the interference angle. However, it was found to be sensitive to alignment. The generation of molten material, which resolidifes during the process, can also be responsible for the dimensional deviation.

The results confirm the feasibility of the approach on a material with low melting point, which is a limiting factor on the applicability of the DLIP process. The tested conditions produced a relatively large period, which was intentional for this first study. The influence of the processing parameters over the pattern definition for smaller periods requires further attention. Future works will be devoted to the reduction of the pattern dimension and evaluation of the principal surface properties.

ACKNOWLEDGMENTS

The authors gratefully acknowledge IPG Italy for their support during this work and the long standing collaboration.

[1]K. M. T. Ahmmed, C. Grambow, and A. Kietzig, Micromachines **5**, 1219 (2014).
[2]A. Malshe, K. Rajurkar, A. Samant, H. N. Hansen, S. Bapat, and W. Jiang, CIRP Ann. Manuf. Technol. **62**, 607 (2013).
[3]F. A. Lasagni and A. F. Lasagni, *Fabrication and Characterization in Micro-Nano Range*, edited by A. Öchsner, H. Altenbach, and L. F. M. da Silva (Springer, New York, 2011), Vol. 10.

[4]Q. Liu, X. Duan, and C. Peng, *Novel Optical Technologies for Nanofabrication*, edited by D. J. Lockwood (Springer, New York, 2014).
[5]B. K. Nayak and M. C. Gupta, Opt. Laser. Eng. **48**, 940 (2010).
[6]A. Lasagni, C. Holzapfel, T. Weirich, and F. Mücklic, Appl. Surf. Sci. **253**, 8070 (2007).
[7]A. F. Lasagni, D. F. Acevedo, C. A. Barbero, and F. Mücklich, Appl. Phys. A **91**, 369 (2008).
[8]B. Voisiat, M. Gedvilas, S. Indrišiunas, and G. Račiukaitis, Phys. Proc. **12**, 116 (2011).
[9]B. Tan and N. R. Sivakumar, J. Opt. A **7**, 169 (2005).
[10]A. Lasagni, C. Holzapfel, and F. Mu, Appl. Surf. Sci. **253**, 1555 (2006).
[11]M. D'Alessandria, A. Lasagni, and F. Mu, Appl. Surf. Sci. **255**, 3210 (2008).
[12]D. Guenther *et al*., Proc. SPIE. **9736**, 973611 (2016).
[13]E. A. Bremus-koebberling, S. Beckemper, B. Koch, and A. Gillner, J. Laser Appl. **24**, 042013 (2012).
[14]A. Kurella and N. B. Dahotre, J. Biomater. Appl. **20**, 5 (2005).
[15]L. Li, N. Mirhosseini, A. Michael, Z. Liu, and T. Wang, Lasers Surg. Med. **45**, 608 (2013).
[16]S. Allegrini, M. Yoshimoto, M. B. Salles, M. Rivellino, F. Allegrini, L. C. Y. Pistarini, F. J. C. Braga, and A. Helena, Appl. Surf. Sci. **307**, 503 (2014).
[17]L. Qin, Q. Zeng, W. Wang, Y. Zhang, and G. Dong, J. Mater. Sci. **49**, 2662 (2014).
[18]M. P. Staiger, A. M. Pietak, J. Huadmai, and G. Dias, Biomaterials **27**, 1728 (2006).
[19]F. Witte, Acta Biomater. **6**, 1680 (2010).
[20]R. Waksman *et al*., Catheter Cardiovasc. Intervention **68**, 607 (2006).
[21]D. Schippman, A. Weisheit, and B. L. Mordike, Surf. Eng. **15**, 23 (1999).
[22]D. Dube, M. Fiset, A. Couture, and I. Nakatsugawa, Mater. Sci. Eng. A **299**, 38 (2001).
[23]J. Dutta Majumdar, R. Galun, B. Mordike, and I. Manna, Mater. Sci. Eng. A **361**, 119 (2003).
[24]R. K. S. Raman, S. Murray, and M. Brandt, Surf. Eng. **23**, 107 (2007).
[25]C. Taltavull, B. Torres, A. J. Lopez, P. Rodrigo, E. Otero, A. Atrens, and J. Rams, Mater. Des. **57**, 40 (2014).
[26]Y. C. Guan, W. Zhou, Z. L. Li, and H. Y. Zheng, J. Phys. D: Appl. Phys. **46**, 425305 (2013).
[27]Y. C. Guan, W. Zhou, Z. L. Li, and H. Y. Zheng, Opt. Lasers Eng. **52**, 35 (2014).
[28]Y. Cui, Surf. Eng. **844**, 1 (2016).
[29]R. G. Li, J. An, and Y. Lu, Surf. Eng. **26**, 347 (2010).
[30]A. G. Demir, V. Furlan, N. Lecis, and B. Previtali, Biointerphases **9**, 029009 (2014).
[31]A. G. Demir, T. B. Taketa, R. Tolouei, V. Furlan, C. Paternoster, M. M. Beppu, D. Mantovani, and B. Previtali, Mater. Lett. **160**, 359 (2015).
[32]V. Furlan, A. G. Demir, and B. Previtali, Opt. Laser Technol. **75**, 164 (2015).
[33]J. Yang, F. Cui, and I. S. Lee, Ann. Biomed. Eng. **39**, 1857 (2011).
[34]A. F. Lasagni, M. Bieda, T. Roch, and D. Langheinrich, Laser Tech. J. **8**, 45 (2011).
[35]S. Housh and B. Mikucki, "Selection and application of magnesium and magnesium alloys," in *Properties and Selection: Nonferrous Alloys and Special-Purpose Materials*, ASM Handbook Vol. 2 (ASM International, Materials Park, OH and Granta Design, Cambridge, UK, 1990), pp. 455–479.
[36]V. Furlan, M. Biondi, A. G. Demir, G. Pariani, A. Bianco, and B. Previtali, Appl. Surf. Sci. **423**, 619 (2017).
[37]M. Born and E. Wolf, *Principles of Optics Electromagnetic Theory of Propagation, Interference and Diffraction of Light* (Cambridge University, London, 2005), pp. 286–409.
[38]H. Hornberger, S. Virtanen, and A. R. Boccaccini, Acta Biomater. **8**, 2442 (2012).